A reversal of climatic trends in the North Atlantic since 2005

Article

Supplemental Material

It is advisable to refer to the publisher's version if you intend to cite from the work. See Guidance on citing.

To link to this article DOI: http://dx.doi.org/10.1038/ngeo2727

Publisher: Nature Publishing Group

www.reading.ac.uk/centaur

CentAUR

A reversal of climatic trends in the North Atlantic since 2005 - supplementary information

Jon Robson,[*] Pablo Ortega and Rowan Sutton

NCAS-Climate, Department of Meteorology, University of Reading

April 20, 2016

This document includes supplementary information and figures for the paper entitled *A recent reversal of climate trends in the North Atlantic.*

1   Sensitivity of 10-year upper-ocean trends

Short linear trends can be sensitive to the chosen start and end points. An obvious question is to what extent is the observed cooling over the North Atlantic over the 2005-2014 period sensitive to inter-annual variability, especially the anomalous winter of the 2013/2014, which exhibited a strong East-Atlantic pattern [1]. We find trends in sea level Pressure (SLP) and sea surface temperature (SST) are sensitive to the inclusion of the winter 2013/2014 (see figure S1). For example, the SST cooling is reduced, and the trend is no longer significant when compared to the inter-annual variability (i.e. the trend is small compared to the residuals), particularly for the 2004-2013 period (see fig. S1 b).

However, the trends in 0-700m average temperature and salinity anomalies (T700 and S700, respectively) are not sensitive to the period over which the linear trend is calculated. Both show significant cooling and freshening over the North East Atlantic (50-10°W, 35-65°N), with warm and salty anomalies along the western boundary (i.e. the east coast of
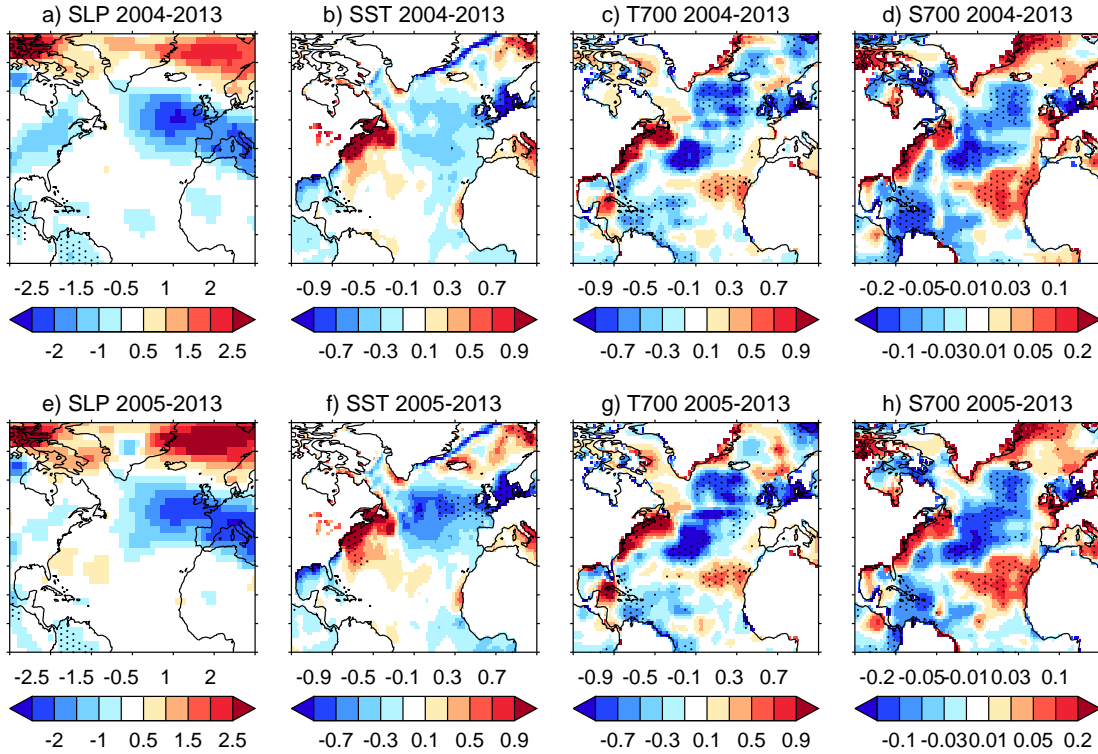
[*]Corresponding author

Figure S1: shows the sensitivity of the recent observed spatial trends to start and end date. a)-d) shows the 10 year trends in SLP, SST, T700 and S700 calculated for the 10 year trend over the period 2004-2013. e) to h) shows the same as a) to d), but now for linear trends calculated over 2005–2013. Stippling shows where trends are significantly different to zero, based on the magnitude of the linear trend being larger than twice the standard error of the residuals (assuming that the residuals are independent). SLP, SST and subsurface ocean data (i.e. T700 and S700) is taken from NCEP reanalysis [2], HadISST [3] and EN4.0.2 [4] datasets respectively.

North America). Note that annual means here are constructed using months December-November, and the cooling of the North East Atlantic is not sensitive to the calculation of annual means from July-June (not shown). Therefore, based on this evidence, we conclude that the large-scale cooling of the North East Atlantic that is discussed in the main paper was not dominated by the anomalous winter of 2013/2014, and instead represents a coherent decadal time-scale change.

2   Anomaly heat budget for North East Atlantic ocean

To further quantify the simultaneous role of the atmosphere, we now construct a simple heat budget. Due to large uncertainties in climatological mean surface flux fields there are large biases in the net heat fluxes from atmospheric reanalysis [5]. Therefore, to quantify the role of surface heat fluxes (SHF) in the cooling of the North East Atlantic region (50–10°W, 35–65°N), we construct an anomaly heat budget based on that used in REF [6].

To calculate the anomaly heat budget we first make monthly mean anomalies of each separate SHF component. Climatological values are computed at each grid-point for each of the surface heat fluxes (latent, sensible, shortwave, longwave) individually by averaging the monthly-mean fields over 1980–2014 (i.e. the satellite record). We use a long period to be confident in the estimation of the monthly varying climatology. The anomalies for each SHF component are then defined relative to the relevant climatology independently. The net surface heat flux anomaly is then defined as the sum of the anomalies for all four surface flux variables [6]. The net SHF anomalies (in $\mathrm{W\,m^{-2}}$) are then integrated over the relevant region to give a time-series of monthly-mean anomalous energy flux (in W). The net SHF anomalies from December 2004 onwards for NCEP [2] and ERA-I [7], integrated over the North East Atlantic (50–10°W, 35N-65°N) are shown in figure S2 a. As discussed by REF [6] (but for a different region) the anomalies of the Net SHF are largely consistent between both NCEP and ERA-Interim giving some confidence in the veracity of the anomalous heat budget.

To get a representative implied heat content anomaly (in Joules) due to surface heat fluxes we then integrate the area-integrated net SHF anomalies in time. For the resultant time-series to be comparable with the actual heat content change an anomaly heat budget makes the strong assumption that the time-mean (i.e. 'climatological') state is associated with a balanced heat budget (i.e. with no changes in net heat content over the time-period used to define the climatology). However, there have been significant changes in North Atlantic heat content (see figure 1 in the main paper). As any errors in the definition of the anomalies will accumulate when calculating the implied heat content change, especially when integrated over long periods [6], we do not simply integrate the

anomalous net SHF, nor do we focus on explaining the full 10-year (or longer) trends. Instead we focus on shorter time-scale variability, and shorter integration periods, by simply asking to what extent did recent winters (i.e. 2013/2014) affect the North East Atlantic (50–10°W, 35N-65°N) heat content. We do this by, first, making the net SHF monthly-mean anomalies relative to the mean anomaly of the 2004–2008 period (i.e. there is no seasonal dependence; we refer to as the "reference" period) and, then, integrating in time from 2004 onwards. The 2004–2008 period is chosen as heat content anomalies remained relatively unchanged (e.g. compared to the 1980s and the 2000s).

Figure S2 c shows the results of the integration for both NCEP and ERA-I surface heat flux (SHF) anomalies. Over the first 5 years of the time-series (i.e. 2004–2008) the anomalies integrate to 0 by construction, and there is little change in the ocean heat content. Following 2008, the integrated SHFs do cause an overall cooling of the region, but it can not explain all of the observed cooling. Although the variability is well correlated between NCEP and ERA-I anomalous heat fluxes, small differences in SHF between data sets highlights the uncertainty in the magnitude of the SHF's role in the cooling. Nevertheless, the analysis of the SHFs suggests that following 2009, that local SHFs contributed $<0.5\times10^{22}$J of cooling - less than 1/3 of the observed cooling over the 2005–2014 period.

As the implied heat content change due to anomalous SHF is dependent on the reference period used, we also explored the sensitivity of these results to the definition of the reference period. Figure S3 shows the same result as that shown in figure S2 c, but now using a range of 5- and 10-year reference periods. Overall, we do find that the implied heat budget change is sensitive to the chosen reference period. This is particularly true when using 5-year reference periods, which are susceptible to the inclusion or omission of extreme years. In the examples in figure S3 the total ocean cooling by 2014 ranges between ~-0.1^{22}J to ~-0.5$\times10^{22}$J (see figure S3), values that are similar for the majority of the reference periods constructed using consecutive years between 1995-2008 (i.e. when the North Atlantic was anomalously warm [8], not shown). We must note, however, that it is possible to construct reference periods where the implied heat content change using NCEP SHFs is ~-0.9^{22}J (i.e. explaining 60% of the observed heat content change), to ~+0.3^{22}J, using the 2003-2007 or 1999-2003 reference periods, respectively (not shown).
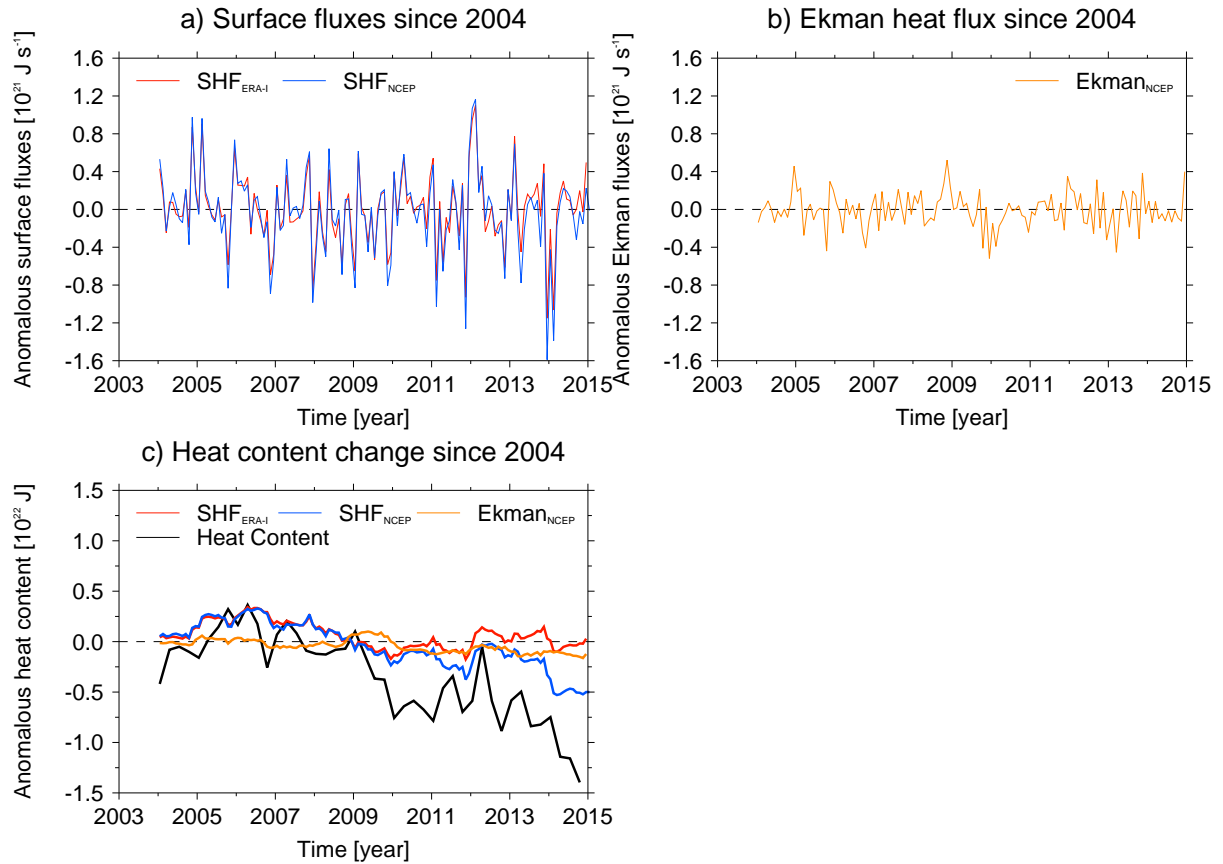
Figure S2: The contribution of surface flux forcing to the observed North Atlantic cooling. a) shows the anomalous monthly-mean net surface flux (since Dec 2004) integrated over the region of cooling (50-10°W,35-65°N), in both ERA-Interim (red) and NCEP (blue) reanalysis products (see text for details). Negative fluxes are cooling the ocean. b) shows the anomalous heat flux associated with the anomalous Ekman upwelling in this region. c) shows the contribution of the anomalous surface fluxes and Ekman upwelling to the most recent period by integrating the anomalous fluxes in time (i.e. cumulatively) after anomalies have been made relative to the 2004-2008 reference period. Finally, the 0-700m ocean heat content change for this region, as measured by the EN4 analysis, is shown in black.

The implied ocean heat content change calculated when using ERA-Interim SHFs is generally less sensitive to the reference period, with a total heat content change between $\sim$-0.4^{22}J, to $\sim$+0.3^{22}J when using the 2003-2007 or 1999-2003 reference periods (not shown). However, the implied ocean heat content change using both NCEP and ERA-Interim is less sensitive when using 10-year reference periods (i.e. compare figure S3 d)-f) with figure S3 a)-c)).

Therefore, we summarise that the implied heat content change calculated from the anomalous SHF is uncertain. However, anomalous SHF does not appear able to explain the entire post-2005 cooling in the North East Atlantic even when using reference periods which produce the most extreme implied heat content changes. Thus, this evidence, taken with the other evidence presented in the main paper (such as the contemporaneous cooling and freshening of the North East Atlantic, as well as the difference in the spatial patterns of anomalous SHF and heat content change), supports our general conclusion that the cooling of the North East Atlantic since 2005 is consistent with a slowdown of the ocean circulation, and related heat transports.

In addition to the SHF we also consider a simple heat budget for the contribution of Ekman upwelling. As the deeper ocean is cooler that the surface ocean, an increase in the amount of Ekman upwelling can lead to a cooling [9]. Therefore, also shown in Figure S2 b is an estimate of the heat flux into the North East Atlantic region due to anomalous Ekman induced upwelling.

We estimate the influence of the anomalous Ekman upwelling by first estimating the Ekman pumping. We make no assumptions here on where the Ekman divergence is occurring in the water column, but instead just focus on the magnitude of the upwelling signal and assume that it is barotropic. We do this by estimating the spatial-average of the monthly-mean upwelling or downwelling velocity (w_{ek}) and multiplying it by the climatological gradient in temperature between the surface and 700m ($d\bar{T}/dz$; i.e. for simplicity we ignore heat content changes in time). The change in upper ocean heat content (0-700m) due to Ekman heat fluxes, defined as $dOHC_{ek}/dt$, is given by the equation below, which is similar to that defined by [10].
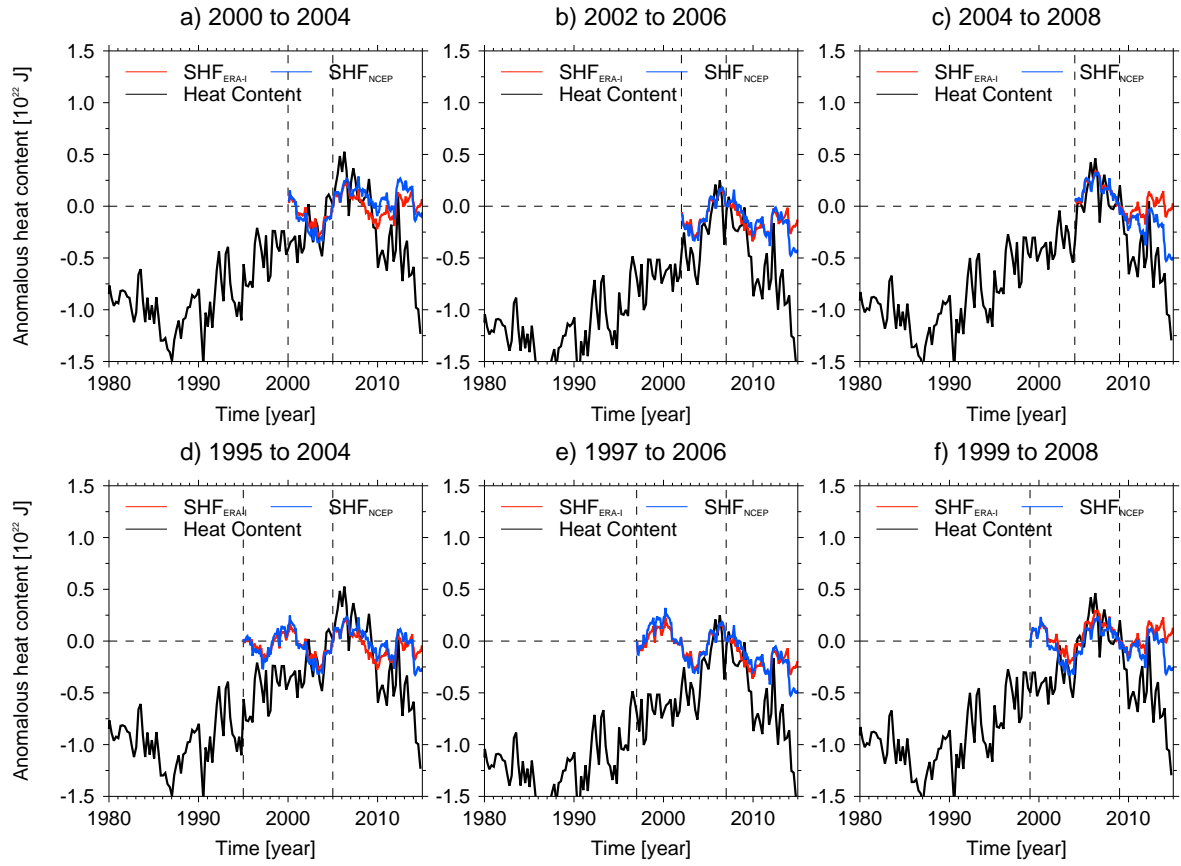
Figure S3: Shows the sensitivity of the implied heat content change to the definition of different reference periods. a) shows the implied heat content change due to anomalous surface fluxes (SHF) by integrating the anomalous SHF in time (i.e. cumulatively) after anomalies have been made relative to the 2000–2004 reference period (which is shown by the vertical dashed lines) for ERA-Interim (red) and NCEP (blue) reanalysis. Observed ocean heat content anomalies over the 1980–2014 period are shown in black and are made relative to the final year in the reference period to highlight the role of SHF in explaining heat content changes that occur after the reference period (i.e. 2004 in the case of a). b) and c) show the same as a) but now when using the 2002–2006 and 2004–2008 reference periods, respectively. d) to f) show the same as a) to c) but for similar 10-year reference periods (1995–2004, 1997-2006 and 1999-2008, respectively). Note that c) is the same as that shown on figure S2, but now with a wider context for the ocean heat content changes.

$$\frac{dOHC_{ek}}{dt} = \rho c_p A \int_0^{700m} w_{ek} \frac{d\bar{T}}{dz}\,dz$$

where ρ is the density of water, c_p is the specific heat capacity at constant pressure, and A is the area of the region of interest. By assuming that w_{ek} is barotropic, and integrating by z we obtain.

$$\frac{dOHC_{ek}}{dt} = \rho c_p w_{ek} A [\bar{T}_{0m} - \bar{T}_{700m}]$$

The climatological period is 1900-2014 for T, which is calculated from EN4, and 1948-2014 for the surface winds from NCEP. Both w_{ek} and $[\bar{T}_{0m} - \bar{T}_{700m}]$ are averaged over the North East Atlantic region first, before calculating $dOHC_{ek}/dt$.

The time-series of monthly-mean $dOHC_{ek}/dt$ is made relative to the climatological seasonal cycle, and finally, the anomalies, $dOHC'_{ek}/dt$, are made relative to the reference period 2005-2009. $dOHC'_{ek}/dt]$ is shown in figure S2 b, and the integration of these fluxes in time is shown in figure S2 c (orange). Although anomalous Ekman upwelling is found to contribute to the overall cooling of the North East Atlantic, the magnitude of the cooling since 2009 is $\sim 0.2 \times 10^{22}$ J, which is $<15\%$ of the total cooling from 2005-2014. Similar numbers are found when using ERA-Interim surface winds (not shown)

3 Consistency of model and observational trends in upper ocean heat content

When comparing the observed spatial ocean heat content trends with those simulated by the HadGEM3-GC2 model [11], it is apparent that they are not the same (compare figure 1 and 3 in the main paper). In particular, the observed cooling of the North East Atlantic covers a larger area (reaching over the North East subtropical gyre between 35-50N), and the observed trends appear to be larger in magnitude. There are many different drivers of heat content variability in the North East Atlantic that is not linked directly to deep Labrador Sea Density anomalies, including atmospheric surface flux changes (due

to the North Atlantic Oscillation, for example [8, 12]) or wind stress curl forced ocean variability [13, 14]. Therefore, to assess whether the differences between the magnitude of the observed and modelled trends in the upper ocean is due to a shortcoming of the model, or a feature of the comparison (i.e. we are comparing 1 large observed event with the average of 9 simulated) we now characterize all the model's trends.

Figure S4 shows the model's time-series of deep Labrador Sea density anomalies (averaged between 1000-2500m), and the 0-700m average temperature (T700) in the Eastern SPG (ESPG, 38-10°W, 50-62.5°N) in the top left panel. These time series highlight the substantial multi-decadal variability seen in both variables in the HadGEM3-GC2 model. The cross-correlation of trends in these time-series is shown in the top right panel, which shows that T700 in the ESPG warms after the density time-series peaks[1]. The peak warming is found at ∼4-6 years, but positive from years 1-12. A similar relationship is seen for the whole North East Atlantic region in figure S5 (50-10°W, 35-65°N)

We choose a lag of 5-years between density and heat content trends (i.e. the the lag with the largest correlation in S4 b) to construct a scatter plot that quantifies the relationship between deep Labrador Sea density and the upper ocean heat content in the ESPG (see figure S4 bottom panels, grey and black crosses). For comparison we also plot the peak observed trends (which is the density trend from 1995-2009, and the T700 trend from 2005-2014, red circle). Figure S4 shows the observed deep Labrador Sea Density trend over 1995-2009 is larger than the internal variability in the HadGEM3-GC2 model, but only marginally so. The observed ESPG T700 cooling trend is also large compared to the modelled variability, but we note that there are larger T700 trends in the model. In the wider North East Atlantic region the observed T700 cooling is larger than any model trend, but there are T700 trends in the model that are only marginally smaller (see figure S5).

We also highlight the trends associated with the 9 independent cases used in the main paper's figure 3. To be more consistent with the observations (where the maximum

---

[1]Note this is a similar relationship to that shown in figure 3 h in the main paper, but now for 10-year trends in T700 in order to compare with the observed cooling. 15 year trends are still used for the deep Labrador Sea density. Additionally, the cross correlation is not inverted in order to highlight the cooling, as was shown in figure 3 e in the main paper.

cooling lags the density by 10 years) we relax the criterion for defining the maximum cooling trend at lag 5. Instead we pick the maximum cooling trend found between lags 1-10 years after the density trend (i.e. consistent with the maximum correlations seen in figure S4 b). These trends are shown in the purple crosses in figure S4, with the mean shown in the purple circle. The trend from the composite analysis further shows that although the trends in the observations is an extreme, it is not inconsistent with modelled variability, particularly in the ESPG (see figure S5).

Therefore, we conclude that although the observed trends would be extreme in this model and are larger than would be predicted by the mean relationship highlighted by the linear-regression between the two variables, they are not inconsistent with the variability simulated within the model. The mean of the model's composite trends is also smaller than the largest individual events used in the composite (compare purple crosses with the purple circle). Therefore, the difference in magnitude between observed and modelled trends is consistent with the comparison method we have used, i.e. we compare a mean of 9 events with one extreme event.

Additionally, we also note that the scatter plot suggests that there may be a non-linearity in the relationship between density trends and upper ocean heat content. Specifically, for extreme density trends (e.g. bigger or smaller than 0.0125 or -0.0125 $kg\,m^{-3}$ per decade, respectively) changes in temperature are above and below the mean-regression line in the scatter plots (blue line), respectively. We test the sensitivity to this by re-calculating the linear regression when only using density trends larger or less than 0.0125 or -0.0125 $kg\,m^{-3}$ per decade (approximately half of the observed density trend), which does support an idea for a weak non-linearity in the relationship (i.e. that the response to deep Labrador Sea Density becomes larger for extreme values of the deep Labrador Sea Density index).

Finally, to put the importance of the winter 2013/2014 in the observations into further context, the red cross on figures S4 and S5 shows the trend for the 2005-2013 period (still expressed as a °C/decade). This comparison further highlights the insensitivity of the oceans heat content trend to the inclusion of 2013/2014, as discussed in section 1.
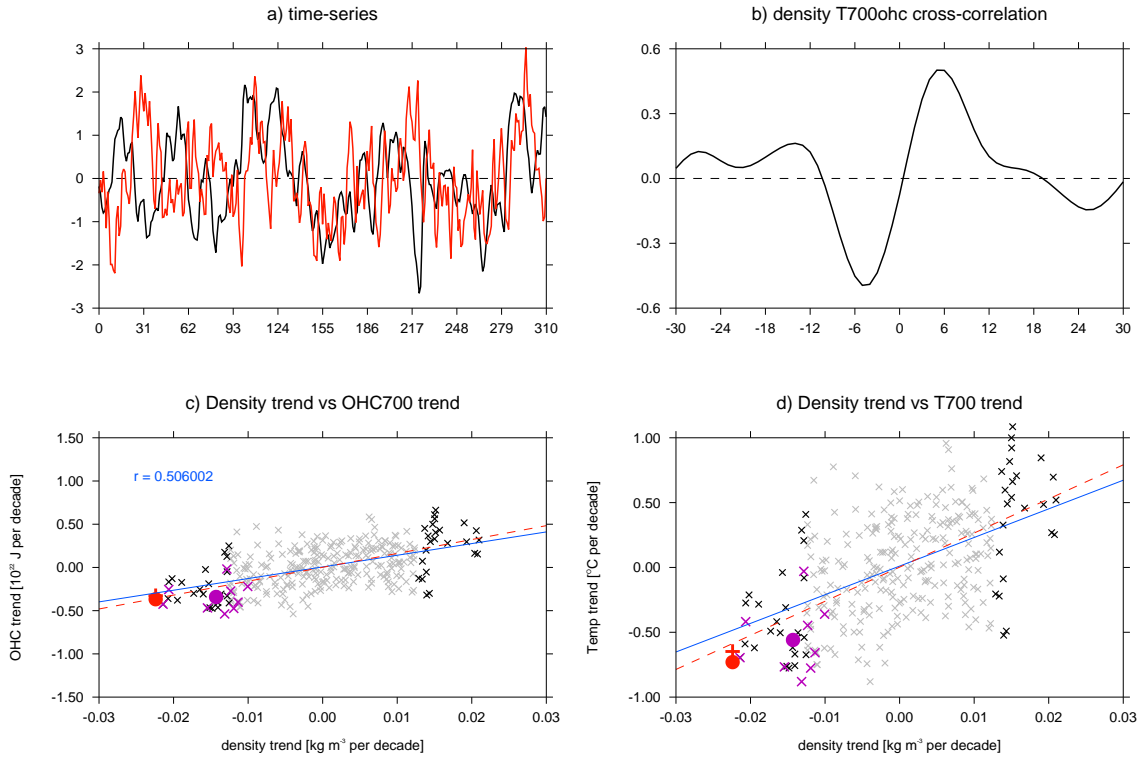
Figure S4: Figure shows a comparison of the magnitude of modelled density and upper ocean heat content trends within the model and the observations. a) shows the time series of 1000-2500m density in the Labrador Sea (black), and the 0-700m average temperature anomaly in the eastern subpolar gyre in the HadGEM3-GC2 model (note that for comparison both time-series have been normalized by their standard deviation). b) shows the cross-correlation of 15-year trends in deep Labrador Sea density with 10-year trends in ESPG T700 heat content trends. c) shows the scatter plot depicting all 15-year deep Labrador Sea density trends, and the 10-year ESPG heat content trends (10^{22} J), where the heat content trends lag the density by 5 years (grey crosses). The red circle is the observed values (using the maximum of both the density trend (1995-2010) and the heat content trend (2005-2014)), the purple circle and crosses show the mean and individual values from the 9 events used to construct figure 3 in the main paper. Note that for the purple crosses, the lag between density and upper ocean heat content is allowed to vary for each event between 1-10 years (see text for details). Finally, the regression between density and heat content changes at a lag of 5 years (using all available data) is shown in the blue line, and only with data where the absolute magnitude is larger than $0.0125 \, \mathrm{kg \, m^3/decade}$. d) shows the same as the c), but is now comparing volume average temperature anomalies (°C).
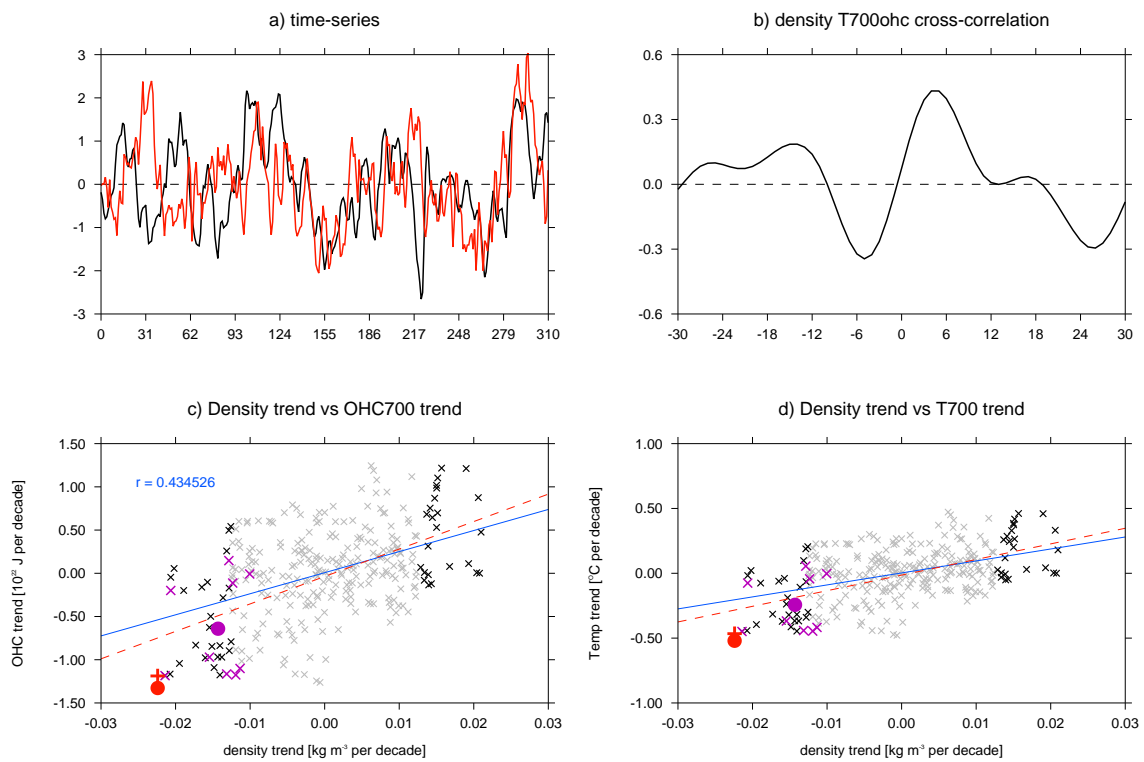
Figure S5: Same as figure S4, but now for the North East Atlantic box (35-65°N, 50-10°W)

4 The influence of the atmosphere on the cooling trends in HadGEM3-GC2

In HadGEM3-GC2 there are also trends in the atmosphere, i.e. the tendency for more positive North Atlantic Oscillation (NAO [15], see figure 3 e in the main paper) that could also contribute to the simulated cooling trends of the North East Atlantic. The increased winds associated with the NAO increase the surface heat loss over the Labrador Sea (fig. S6), but the surface fluxes are not found to exert a strong cooling of the ESPG. Indeed, surface fluxes are acting to warm a substantial area of the ESPG (fig. S6). Therefore, this comparison of the spatial pattern of the SHF trends would suggest that the large cooling trends in the ESPG following a decrease in deep Labrador Sea density in this model cannot be explained by the trend to positive NAO. This suggests that ocean circulation changes are dominant in the ESPG in the model, and is also consistent with the reduction in the AMOC seen in figure 3 e.
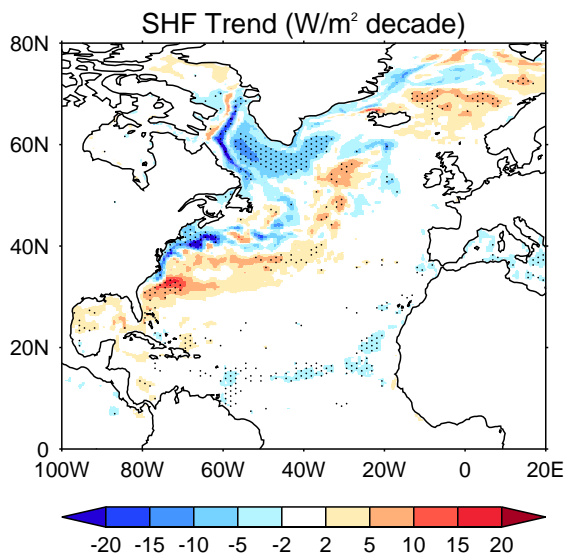

Figure S6: Composite of simulated 15-year linear trend in total surface heat fluxes (SHF, [$W\,m^{-2}$/Decade]) following a reduction in Labrador sea deep density index in the HadGEM3-GC2 model. The analysis is the same as that for figure 3 in the main manuscript. The composite is based on the 9 largest independent decreases in deep Labrador Sea density, and the trend in SHF lags the trend in density by 5 years. Negative trends show where the ocean is being cooled.

5 Water mass changes controlling deep Labrador Sea Density

In the main paper figure 1, we showed that density in the deep Labrador Sea has reached record low values in 2014. Although there is clearly uncertainties in the size of density anomalies in the past due to a lack of data [4], the question arises, why has the decrease in density in the region been so large? To attempt to answer this we decompose the water mass changes that have driven the changes in density.

Figure S7 shows that the decrease in density since 1995 is associated with a warming and a salinification trend of deep Labrador Sea water masses; hence, deep Labrador Sea density is temperature dominated overall. However, taking the observed data at face value note that, *i)*, the temperature is not (yet) warmer than that observed in the late 1960s/early 1970s (the previous low in observed density anomalies), which could be seen as a surprise given the expected influence of Anthropogenic forcing on global upper-ocean temperatures over this period [16, 17]. Additionally, *ii)*, the deep Labrador Sea is fresher than it was in the late 1960s/early 1970s. Therefore, the data suggests that freshening of the deep ocean, relative to the late 1960s, has been an important factor in creating the record low densities in this region.
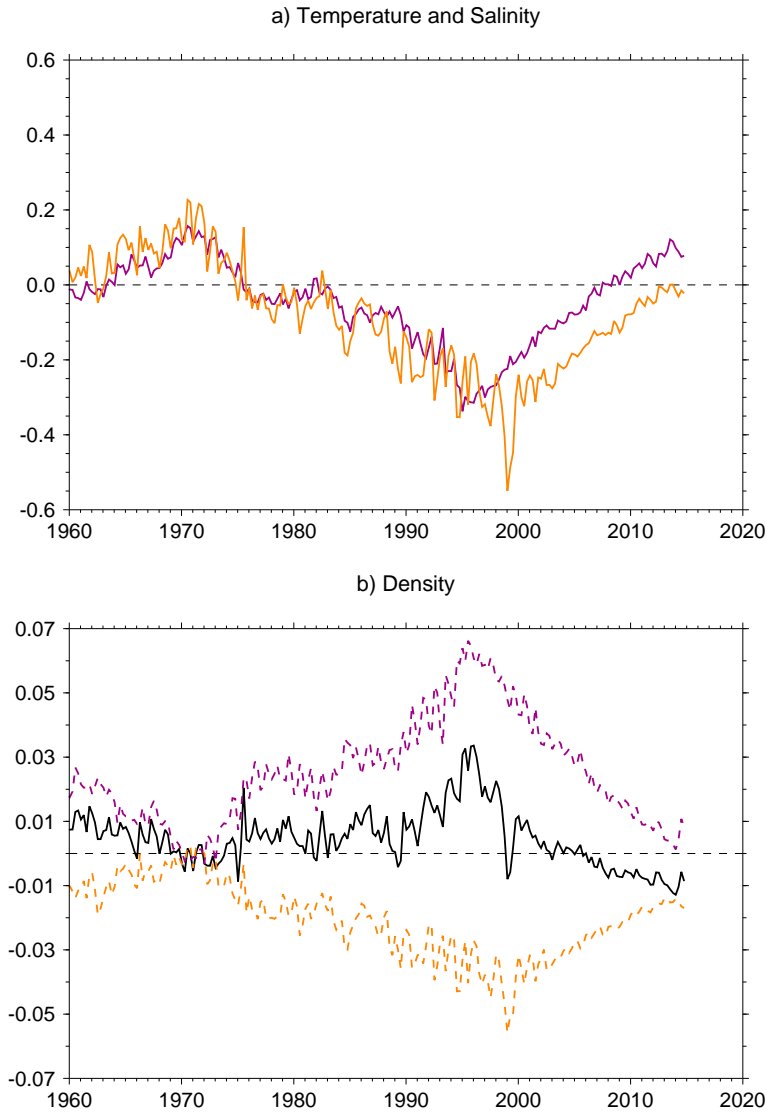
Figure S7: Water-mass changes in the deep Labrador Sea. a) shows the 1000-2500m volume-averaged temperature (purple, [°C]) and salinity (orange, [PSU×10]) seasonal-mean anomalies from the Labrador Sea (60°W-35°W, 50°N-65°N). Anomalies are expressed relative to the seasonal-means for the 1961-1990 period. b) shows the resultant density anomalies (black, [kg m^{-3}], where density is relative to 2000m i.e. σ_2. Also shown for reference is the contribution of the density change due to temperature (purple) and salinity changes (orange) which is calculated by holding salinity and temperature at values observed in 1971, respectively. For comparison, all density time-series are made relative to the time-mean of 1971 (approximately the previous minimum in observed deep Labrador Sea density).

References

[1] Grist, J. P. *et al.* Extreme air–sea interaction over the north atlantic subpolar gyre during the winter of 2013–2014 and its sub-surface legacy. *Climate Dynamics* 1–19 (2015).

[2] Kalnay, E. *et al.* The NCEP/NCAR 40-year reanalysis project. *Bulletin of the American Meteorological Society* **77**, 437–471 (1996).

[3] Rayner, N. *et al.* Global analyses of sea surface temperature, sea ice, and night marine air temperature since the late nineteenth century. *Journal of Geophysical Research-Atmospheres* **108**, 4407 (2003).

[4] Good, S. A., Martin, M. J. & Rayner, N. A. En4: quality controlled ocean temperature and salinity profiles and monthly objective analyses with uncertainty estimates. *Journal of Geophysical Research: Oceans* **118**, 6704–6716 (2013).

[5] Josey, S., Gulev, S. & Yu, L. Exchanges through the ocean surface. In Sidler, G., Griffies, S., Gould, J. & Church, J. (eds.) *Ocean Circulation and Climate: A 21st Century Perspective* (Academic Press, 2013).

[6] Cunningham, S. A. *et al.* Atlantic meridional overturning circulation slowdown cooled the subtropical ocean. *Geophysical Research Letters* **40**, 6202–6207 (2013).

[7] Dee, D. *et al.* The era-interim reanalysis: Configuration and performance of the data assimilation system. *Quarterly Journal of the Royal Meteorological Society* **137**, 553–597 (2011).

[8] Robson, J., Sutton, R., Lohmann, K., Smith, D. & Palmer, M. Causes of the Rapid Warming of the North Atlantic ocean in the mid 1990s. *J Clim.* **25**, 4116–4134 (2012).

[9] McClain, C. R. & Firestone, J. An investigation of ekman upwelling in the north atlantic. *Journal of Geophysical Research: Oceans (1978–2012)* **98**, 12327–12339 (1993).

[10] Marshall, J. C., Williams, R. G. & Nurser, A. G. Inferring the subduction rate and

period over the north atlantic. *Journal of Physical Oceanography* **23**, 1315–1329 (1993).

[11] Williams, K. *et al.* The Met Office Global Coupled model 2.0 (GC2) configuration. *Geoscientific Model Development Discussions* **8**, 521–565 (2015).

[12] Menary, M. B., Hodson, D. L., Robson, J. I., Sutton, R. T. & Wood, R. A. A mechanism of internal decadal atlantic ocean variability in a high-resolution coupled climate model. *Journal of Climate* **28**, 7764–7785 (2015).

[13] Häkkinen, S., Rhines, P. B. & Worthen, D. L. Warm and saline events embedded in the meridional circulation of the northern North Atlantic. *Journal of Geophysical Research* **116**, C03006 (2011).

[14] Häkkinen, S., Rhines, P. B. & Worthen, D. L. Atmospheric blocking and atlantic multidecadal ocean variability. *Science* **334**, 655–659 (2011).

[15] Hurrell, J. W. Decadal Trends in the North Atlantic Oscillation: Regional Temperatures and Precipitation. *Science* **269**, 676–679 (1995).

[16] Domingues, C. M. *et al.* Improved estimates of upper-ocean warming and multi-decadal sea-level rise. *Nature* **453**, 1090–1093 (2008).

[17] Levitus, S. *et al.* Global ocean heat content 1955-2008 in light of recently revealed instrumentation problems. *Geophys. Res. Lett.* **36** (2009).